Proceedings of the 10th Brazilian Congress of Thermal Sciences and Engineering – ENCIT 2004
Braz. Soc. of Mechanical Sciences and Engineering – ABCM, Rio de Janeiro, Brazil, Nov. 29 – Dec. 03, 2004

Paper CIT04-0211

DEVELOPMENT AND ANALYSIS OF A MESH REFINEMENT/COARSENING PROCEDURE FOR GAS DYNAMIC PROBLEMS

Miguel T. Walter, Aline A.Q. Abdu, Luís Fernando Figueira da Silva
Department of Mechanical Engineering
Pontifícia Universidade Católica do Rio de Janeiro
Rua Marquês de São Vicente, 225
22453-900 Rio de Janeiro, RJ, BRAZIL
matwalter@hotmail.com, alineabdu@yahoo.com.br, luisfer@mec.puc-rio.br

J.L.F. Azevedo
Centro Técnico Aeroespacial
CTA/IAE/ASE-N
12228-900, São José dos Campos, SP, BRAZIL
azevedo@iae.cta.br

Abstract. *The compressible gas flows of interest to aerospace applications often involve situations where shock and expansion waves are present. Decreasing the characteristic dimension of the computational cells in the vicinity of shock waves improves the quality of the computed flows. This reduction in size may be accomplished by the use of mesh adaption procedures. In this paper an analysis is presented of an adaptive mesh scheme developed for an unstructured mesh finite volume upwind computer code. This scheme is taylored to refine or coarsen the computational mesh where gradients of the flow properties are respectively high or low. The refinement and coarsening procedures are applied to the classical gas dynamic problems of the stabilization of shock waves by solid bodies. In particular situations where oblique shock waves interact with an expansion fan and where bow shocks arise around solid bodies are considered. The effectiveness of the scheme in reducing the computational time, while increasing the solution accuracy, is assessed. It is shown that the refinement procedure alone leads to a number of computational cells which is 20% larger than when alternate passes of refinement and coarsening are used. A reduction of computational time of the same order of magnitude is obtained when coarsening of the mesh is performed.*

keywords: *Mesh adaption, unstructured meshes, compressible flows, numerical methods*

1. Introduction

Mesh adaption procedures are frequently used to reduce the characteristic dimension of the computational cells in interesting regions of the flowfield, with the aim of yielding a better resolution of the simulated phenomena. Most often in computational fluid dynamics, these regions are those where the gradients of the flow properties are high or where the numerical solution exhibits a large error. Typical regions of high gradients are boundary and shear layers, chemical reaction fronts and shock waves. An accurate computation of these regions is required in order to predict aero and thermodynamical loads. However, the exact position of these regions are not known *a priori*. In particular, shock waves are usually captured by the discretization schemes of the governing equations and span over two or three computational cells, even though the physical dimension of these waves is of order of a few mean free paths of the gas molecules. Successive refinements are usually necessary to achieve a good resolution of the regions of the flowfield where high gradients occurs. As a consequence, a significant increase in the number of mesh volumes may result, eventually leading to a concentration of refined volumes in regions of the flowfield where those volumes are no longer needed. Thus, mesh coarsening techniques are of interest with the aim of increasing the characteristic dimension of the computational mesh, ultimately leading to a reduction of the computational time.

In this paper, refinement and coarsening techniques taylored for unstructured meshes are evaluated with respect to the gains in solution accuracy and computational time. During the past few years, several authors have developed mesh adaption techniques in an unstructured mesh context.

Hierarchical mesh adaption techniques have been developed (Kallinderis and Vijayan, 1993; Speares and Berzins, 1997) on three-dimensional unstructured meshes. The coarsening procedure acts only in regions previ-

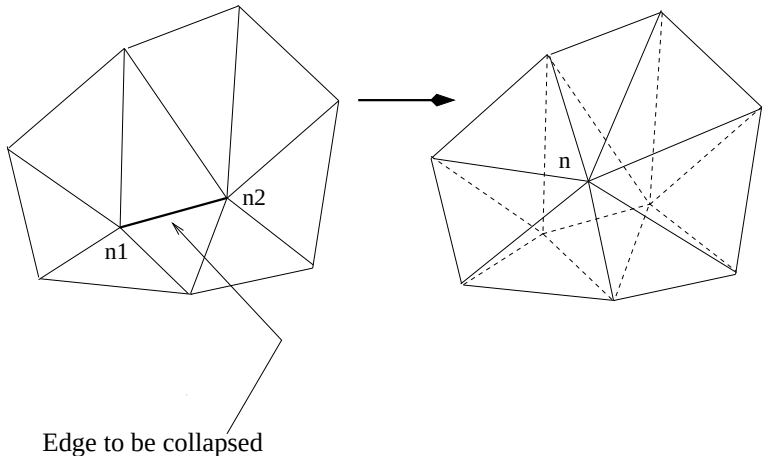

Figure 1: Coarsening scheme using the edge-collapsing procedure.

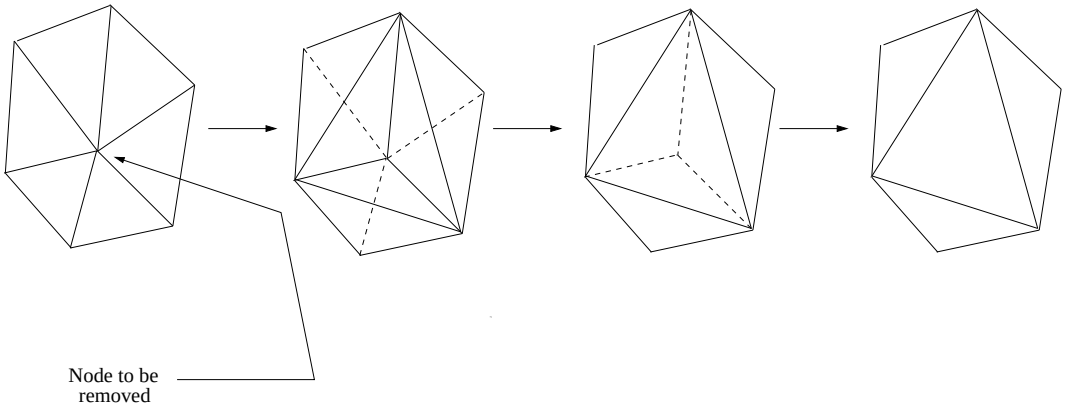

Figure 2: Diagonal swap coarsening procedure scheme.

ously refined, and thus the coarsest mesh possible is the original mesh. Therefore, the largest spatial scales are fixed by the choice of the initial mesh.

Dompierre et al., 2000; Webster et al., 1994 have developed a technique based on the collapse of edges in order to coarsen unstructured meshes in two-dimensional configurations. In this method, the nodes which define a given edge are transformed in one node, and the volumes around the removed edge cease to exist. Figure 1 provides a schematic representation of this situation.

While the former method is better suited for the simulation of transient phenomena, since the initial mesh can be recovered at any time, the latter is more indicated to the simulation of steady state problems. Moreover, the edge-based data structure used in the computer code adopted in the present work is ideally suited to the edge-collapse technique.

Miller et al., 1999 developed a coarsening approach for two-dimensional unstructured meshes which leads to a sequence of bounded aspect ratio meshes, i.e., meshes for which all elements have bounded aspect ratios. This procedure guarantees that both the number of meshes in the sequence and the number of elements on a given mesh are optimal.

Another procedure, which may be used to coarsen the mesh, begins with the choice of one node to be removed. As illustrated in Fig. 2, around this node, a diagonal swap technique is applied, in order to end up with only three edges sharing this node. These edges are removed, together with the three adjoining triangles, and a new triangle is formed.

Still another possibility, which has not been explored in the litterature, to the best of the authors' knowledge, is the use of Delaunay triangulations to reconstruct regions of the mesh where triangles have been removed. This procedure does not necessarily lead to an increase of the characteristic dimension of the mesh. Moreover, the Delaunay triangulation complicates the attribution of properties from the original mesh to the new one.

Sophisticated implementations could be devised, which would combine two or more of the techniques briefly

described here, with the aim of optimizing the mesh quality. However, defining these implementations is beyond the scope of the present work.

After recalling the mathematical formulation for 2-D gas dynamic problems, and the associated numerical method, this paper describes in detail the mesh coarsening procedure developed. Then, the refinement and the coarsening procedures are evaluated by means of computations of compressible gas flow problems.

2. Theoretical Formulation

In present case, the flowfield is simulated using the 2-D Euler equations, which can be written in the integral conservative form for a 2-D coordinate as

$$\iint_V \frac{\partial \boldsymbol{U}}{\partial t}\, dxdy + \int_S (\boldsymbol{F}\, dy - \boldsymbol{G}\, dx) = 0\,. \tag{1}$$

The vector of conserved quantities, $\boldsymbol{U}$, the expressions for the convective flux vectors, $\boldsymbol{F}$ and $\boldsymbol{G}$, are written as

$$\boldsymbol{U} = \begin{bmatrix} \rho \\ \rho u \\ \rho v \\ \rho E \\ \rho Y_1 \\ \rho Y_2 \\ \vdots \\ \rho Y_{N-1} \end{bmatrix}, \quad \boldsymbol{F} = \begin{bmatrix} \rho u \\ \rho u^2 + p \\ \rho uv \\ u(\rho E + p) \\ \rho Y_1 u \\ \rho Y_2 u \\ \vdots \\ \rho Y_{N-1} u \end{bmatrix}, \quad \boldsymbol{G} = \begin{bmatrix} \rho v \\ \rho uv \\ \rho v^2 + p \\ v(\rho E + p) \\ \rho Y_1 v \\ \rho Y_2 v \\ \vdots \\ \rho Y_{N-1} v \end{bmatrix}. \tag{2}$$

The nomenclature used in this system of equations is the one usually adopted in aerospace applications, such that ρ is the density, u and v are the Cartesian velocity components in directions x and y, E is the total energy per unit of mass, Y_i is the mass fraction of the i-th species, and p is the static pressure.

In the solution of the equation system (1), $N-1$ chemical species are necessary, since the mass fraction of the last chemical species, Y_N, is calculated as $Y_N = 1 - \sum_{i=1}^{N-1} Y_i$. The state equation for a mixture of thermally perfect gases,

$$p = \rho \mathcal{R} T \sum_{i=1}^{N} \frac{Y_i}{W_i}\,, \tag{3}$$

is used to evaluate the pressure, p. In this equation, T is the temperature, $\mathcal{R}$ is the universal gas constant and W_i is the molecular weight of species i. The total energy, E, is defined as the sum of the internal energy, e, and the kinetic energy,

$$E = e + \frac{1}{2}\left(u^2 + v^2\right) = \sum_{i=1}^{N} Y_i e_i + \frac{1}{2}\left(u^2 + v^2\right) = \sum_{i=1}^{N} Y_i h_i - \frac{p}{\rho} + \frac{1}{2}\left(u^2 + v^2\right)\,, \tag{4}$$

The internal energy is a function of the mixture composition and of the temperature, T, which is calculated by a Newton method once e is known. Note that, although the formulation above is pertinent to variable mixture composition flows of interest to previous studies (Figueira da Silva et al., 2000; Pimentel et al., 2002; Walter and Figueira da Silva, 2004), the results presented here consider air as the working fluid.

3. Numerical Method

Computations are performed using a numerical code (Figueira da Silva et al., 2000) that solves the governing equation system (1-2) using an upwind cell-centered finite volume method on unstructured triangular meshes. Temporal discretization uses a classical, 2nd-order, Runge-Kutta time stepping scheme (Mavriplis, 1988). In the spatial discretization, the interface fluxes are formulated using the Advection Upstream Splitting Method (AUSM$^+$, Liou, 1996). Spatial higher order accuracy is sought with MUSCL (Hirsch, 1990) extrapolation. This code has been validated against analytical and experimental results for several compressible gas flows (Figueira da Silva et al., 1999; Figueira da Silva et al., 2000; Pimentel et al., 2002; Walter and Figueira da Silva, 2004).

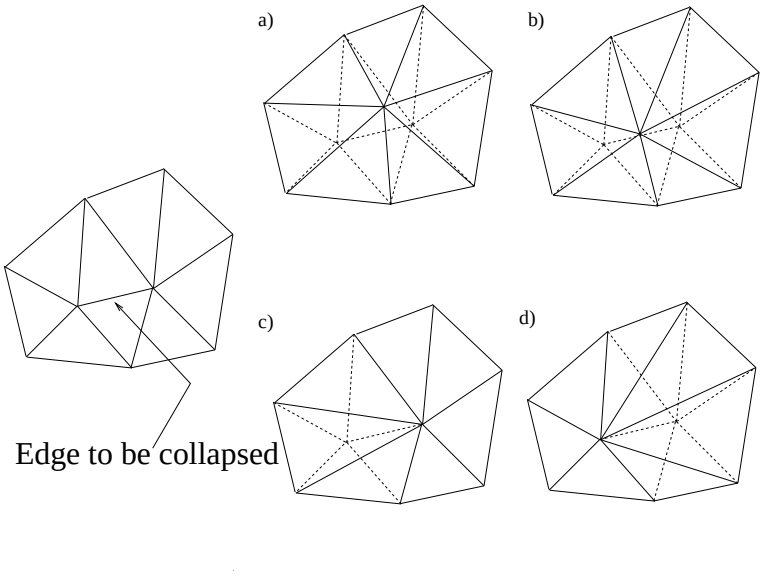

Figure 3: Representation of the four different possibilities of the edge collapse.

4. Adaptive Refinement

The adaptive mesh refinement technique used (Figueira da Silva et al., 2000) increases the number of grid points in regions of the flowfield where large property gradients occur. This procedure requires the identification of such regions, which is accomplished based on a sensor quantity defined for each computational cell

$$(\text{sensor})_i = \max_m \left(\frac{|\nabla \zeta_m|_i}{|\zeta_{m_{\max}} - \zeta_{m_{\min}}|} \right) \quad ; \quad \zeta_m = (p, u, v, T, Y_j) \,, \tag{5}$$

where $\zeta_{m_{\max}}$ and $\zeta_{m_{\min}}$ are the maximum and the minimum values of the ζ_m property in the whole flowfield and $|\nabla \zeta_m|_i$ is the magnitude of the gradient of the ζ_m property in the i-th control volume. As described in greater detail elsewhere (Figueira da Silva et al., 2000), the refinement procedure halves the faces of each volume for which the sensor exceeds a prescribed threshold. The new node created is connected either to existing or to new nodes, leading to the formation of two or four smaller triangles, respectively. Successive refinements are typically used to obtain an adequate resolution of shock or detonation waves (Figueira da Silva et al., 2000; Pimentel et al., 2002; Walter and Figueira da Silva, 2004). However, as several passes of refinement are used, and flow discontinuities steepen, regions of the flowfield may arise where an unnecessary concentration of computational volumes appears. This drawback of the application of the refinement process to the problems of interest to the authors prompted the development of the following coarsening procedure.

5. Coarsening Procedure

The coarsening procedure used in this work is based on the edge collapse technique, illustrated in Fig. 1. This procedure consist on the collapse of two adjoining nodes (n_1 and n_2), leading to the formation of a new node (n). As a result of this procedure, the two neighboring volumes are removed.

5.1. The node removal process

Equation (5) is used to calculate the normalized gradients of the selected variables in the computational domain, starting with the computed results on the initial mesh. The gradients on the edges are calculated as the average of the gradients of the neighboring volumes of a given edge. The edges which have a low value of the normalized gradient are chosen as possible candidates to be removed. These nodes are ordered in a list by increasing values of the gradient. The selected edge removal will occur only if the new mesh quality would not be reduced, when compared to the original one. The mesh quality measure will be discussed further on.

Note that the quality of resulting volumes depends on the position of the new node. As shown in Fig. 3, the procedure considers the following positions:

1. The geometric center of the polygon formed by all volumes surrounding a node [Fig. 3 (a)].

2. The center of the edge to be collapsed [Fig. 3 (b)].

3. Each one of the two original nodes of the edge [Fig. 3 (c, d)].

The position which leads to the best quality of the modified volumes will be chosen. If none of these locations yields a good mesh quality, this edge is deleted from the list of edges to be removed.

Once an edge has been chosen for removal, and with the purpose of avoiding an excessive growth of the volumes, it is enforced that no edges of the same volume will be chosen for removal in the current coarsening pass. As a consequence, a given node is not allowed to be displaced twice during a pass of the coarsening procedure. This restriction defines a domain of influence corresponding to the edge that will be removed, as shown in Fig. 4. All the neighboring edges of one node that has an edge selected to be removed are deleted from the list of edges to be removed, regardless of the value of the sensor.

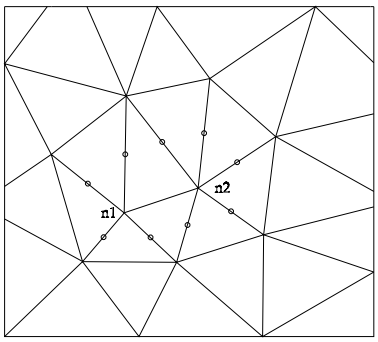

Figure 4: Influence domain of the collapsed edge.

Special care is needed for coarsening volumes along a computational boundary. The present procedure does not consider the removal process in boundary edges, since the code does not contain geometric information about the boundaries. Furthermore, for the edges that have only one node at the boundary, the only possible result would be the collapse to the boundary node, since the edges which define the contour cannot be changed. Therefore, the current implementation does not consider the collapse of edges which have at least a node at the boundary, since it would not lead to a significant increase of the characteristic length scale of the computational mesh. One should note that the drawback related to fixing the edges which concour to a boundary is not large, as the number of edges at the boundaries is much smaller than those at the interior of the computational domain, at least for the cases of interest in this work.

Once the node removal process is finished, the mesh data structure has been modified, leading to the absence of nodes and volumes. In the present context of cell-centered finite volume method, reordering and renumbering the position, connectivity, neighboring and boundary volume tables is necessary. The attribution of the new volume properties occurs, simultaneously, as the volume reordering proceeds.

The ordering process uses two types of lists. The first one is the list of removed nodes, which has dimension equal to 2φ and increasingly orders the removed nodes (n_1 e n_2). The second is the new node list, with dimension φ, which has the number of each new node (n) and the number of the volumes which share those vertices. One should note that the number of the new nodes is half the number of removed nodes. The reordering position table is created by direct attribution of the number of the first φ removed nodes to the new nodes, with simultaneous update of the coordinates. For the last φ nodes, starting by the last element of the list of removed nodes, a shift up movement has to be executed. The reconstruction of the neighborhood table and boundary volume table is performed using both the position reordering table and the connectivity table.

5.2. The quality measure

In this work, the quality of the volumes is a measure of the elongation of the triangles, defined as the ratio of the radius of the inscribed and circumscribed circles

$$Q_\Delta = 2\frac{r}{R}, \tag{6}$$

where r and R are the radius of the inscribed an circumscribed circles by the triangle, respectively, as shown in [Fig. 5 (a)]. The quality criterion adopted in the mesh coarsening procedure is defined by

$$C \leq Q_{\Delta} \leq 1. \tag{7}$$

It should be noted that, for an equilateral triangle [Fig. 5 (b)] $Q_{\Delta} = 1$. The value of the constant C indicates the minimum quality value accepted. Good results have been obtained with C around $0.70 - 0.75$.

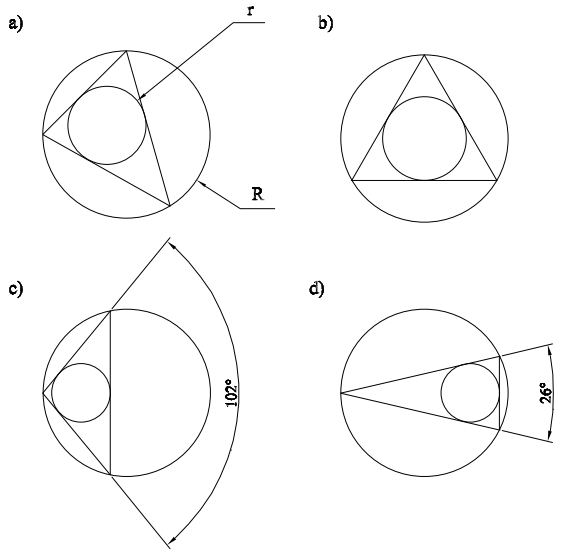

Figure 5: Scheme of volumes with different values of Q_{Δ}.

As an illustration of this metric, note that isosceles triangles with angles equal to 26^0 and 102^0, shown in Fig. 5 (c, d), respectively, both have values of quality $Q_{\Delta} = 0.70$.

6. Results and Discussion

The mesh adaption procedure has been tested in three supersonic airflow configurations. First, the supersonic flow around a hemisphere is considered. The second configuration involves the stabilization of an oblique shock wave (OSW) over a compression ramp, whereas the third considers a ramp of finite length which leads to the interaction between the OSW and an expansion fan.

For the three cases presented here, the results obtained with a coarse mesh are compared to those (i) when three passes of the adaption procedure are performed after convergence of the computations and (ii) when, in addition to these three refinement passes, mesh coarsening is performed a few interactions prior to refinement.

6.1. Supersonic Flow around a Hemisphere

The countours of Mach number obtained for the air flow around a hemisphere using, as freestream parameters, $M_{\infty} = 5$, $p_{\infty} = 1$ atm and $T_{\infty} = 293$ K, are shown in Fig. 6. The corresponding final meshes are also shown in this figure. With the exception of the results shown in Fig. 6 (a), that were obtained with the initial mesh, which is composed of 210 nodes and 360 volumes, the computations involved three refinement passes. For each refinement pass, the threshold value of Eq. (5) is 0.05. Two mesh coarsening passes were also used to obtain the results shown in Fig. 6 (c) and (d). The difference between these two computations lie at the proximity, in terms of the number of interactions of the refinement and coarsening passes. In the cases of Fig. 6 (b) and (d) the refinement passes were performed after 400, 1300 and 3000 interactions, i.e., after complete converence of the solution was observed, whereas the result of Fig. 6 (c) was obtained for refinements performed at 400, 600 and 800 interactions, these small intervals allow only for an overall settling of the solution. The coarsening passes were performed at interactions 500 and 700, in the case of Fig. 6 (c), and 1200 and 1900, Fig. 6 (d), respectively.

The resulting number of nodes and volumes is (1368, 2631), (1320, 2522), (1319, 2520) for the cases shown in Fig. 6 (b), (c) and (d), respectively. As it could be expected, the mesh coarsening procedure leads to a smaller

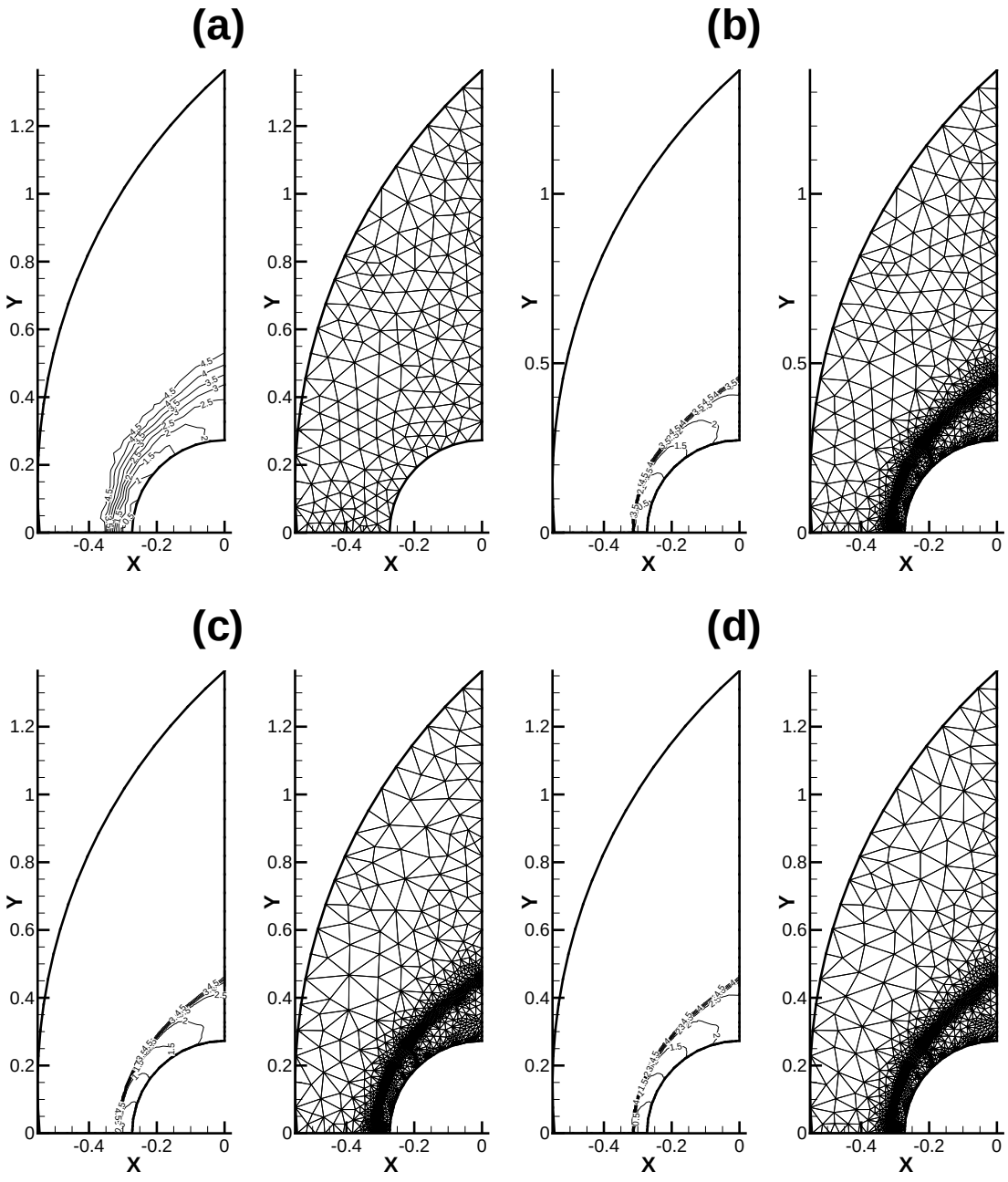

Figure 6: Mesh and Mach number fields corresponding to the airflow around a hemisphere, for different mesh adaption strategies, $M_\infty = 5$, $T_\infty = 293$ K and $p_\infty = 1$ atm.

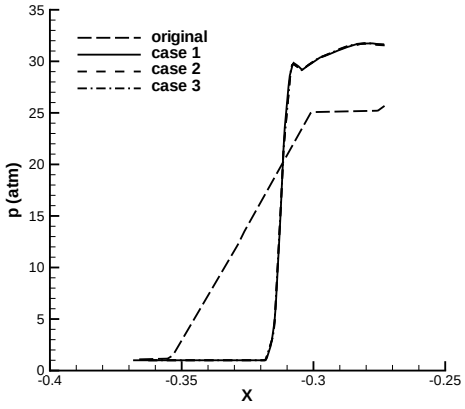

Figure 7: Pressure (atm) evolution along the symetry axis, for different mesh adaption strategies, $M_\infty = 5$, $T_\infty = 293$ K and $p_\infty = 1$ atm.

number of computational volumes and nodes. However, the modest decrease obtained is due to the small value of the threshold used, 10^{-10}, which leads to coarsening of the computational mesh in the freestream region only.

Concerning now the solution accuracy, the inspection of Fig. 6 clearly reveals the gains obtained when refinement is used. The different adaption strategies used are found not to influence the computed result. The increase in solution accuracy can also be assessed by examining the pressure evolution along the symmetry axis, which is shown in Fig. 7. Not only a significant steepening of the pressure jump across the shock wave is obtained after mesh refinement, but also the value of the pressure downstream the normal shock wave, 29 atm, which could not be recovered with the coarse mesh, is now correctly predicted. This figure also shows that mesh coarsening does not affect the solution accuracy.

6.2. Two-Dimensional Supersonic Wedge

Figure 8 gives the results of the computations performed for the second configuration using, as freestream parameters, $M_\infty = 2.25$, $T_\infty = 300$ K and $p_\infty = 1$ atm. The value of the wedge angle is $\delta = 20°$. In this figure are shown the resulting meshes and the pressure contours. The value of the sensor threshold used in all refinement passes is 0.01, whereas the coarsening procedure uses 0.75. Note that mesh adaption is performed after convergence of the computation is obtained on a given mesh. The initial mesh, which is shown in Fig. 8 (a), contains 751 nodes and 1391 volumes. The mesh which results from three refinement passes is shown in Fig. 8 (b), and has 3630 nodes and 7120 volumes. In this case, the total computational time is 6.0 hours. The mesh and the solution corresponding to three refinement and two coarsening passes is given in Fig. 8 (c). The final number of nodes and volumes is 2843 and 5552, respectively, and the total CPU time is 4.8 hours. Note that this duration includes the elapsed time during the refinement and coarsening passes. Thus, the use of mesh coarsening, in addition to mesh refinement, led to a reduction of 22 % in the number of volumes and of 20 % in the CPU time, when compared to using mesh refinement alone. This decrease, much larger than the one obtained in the hemisphere computations, is due to the larger value of the coarsening threshold used.

6.3. Supersonic Finite Ramp

The results obtained for the finite ramp configuration are shown in Fig. 9. The ramp used has an angle of $\delta = 40°$, and the freestream flow parameters are $M_\infty = 8$, $T_\infty = 300$ K and $p_\infty = 1$ atm. In this figure are shown the final mesh and pressure fields for the initial mesh, for the case of three refinement passes and for the case where two coarsening passes preceed the last two refinements. The values of the threshold used in the refinement and coarsening passes is the same as those used in the wedge cases. The initial mesh, shown in Fig. 9 (a) contains 1105 nodes and 2065 volumes, whereas the mesh resulting from three refinement passes, which is depicted in Fig. 9 (b), contains 6500 nodes and 12798 volumes. The total CPU time in the latter case is 8.5 hours. Figure 9 (c) gives the results obtained when two coarsening passes are also performed. The final mesh, for which the total computational time was 6.9 hours, has 5262 nodes and 10322 volumes. In this case, the resulting reduction in CPU time is 18.8 %, and the number of volumes is decreased by 19.3 %.

The computed flow solution is not affected by the coarsening procedure, as it could be expected. This

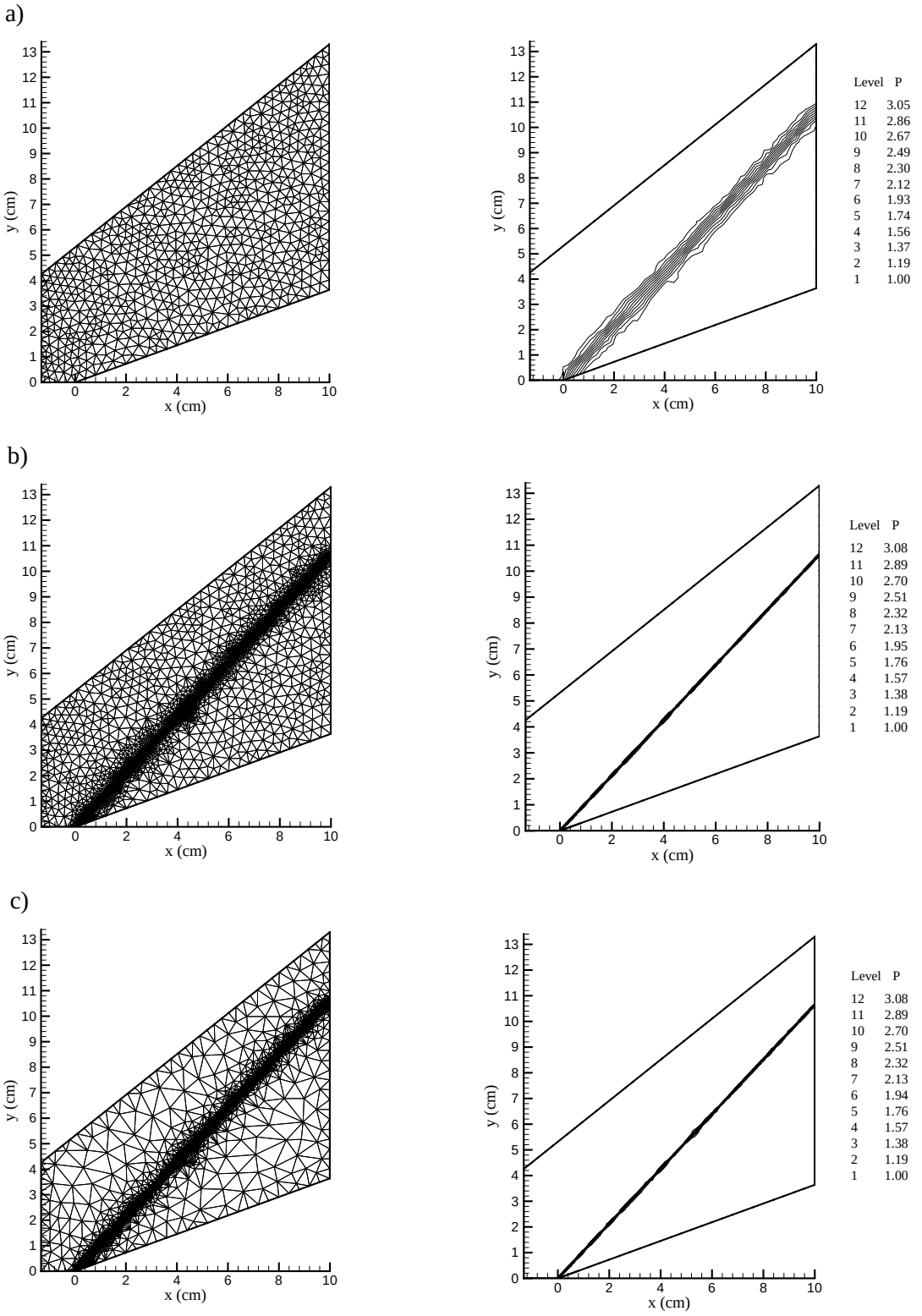

Figure 8: Mesh and pressure field (atm) corresponding to the airflow around a compression ramp, $M_\infty = 2.25$, $T_\infty = 300$ K and $p_\infty = 1$ atm, wedge angle $\delta = 20°$.

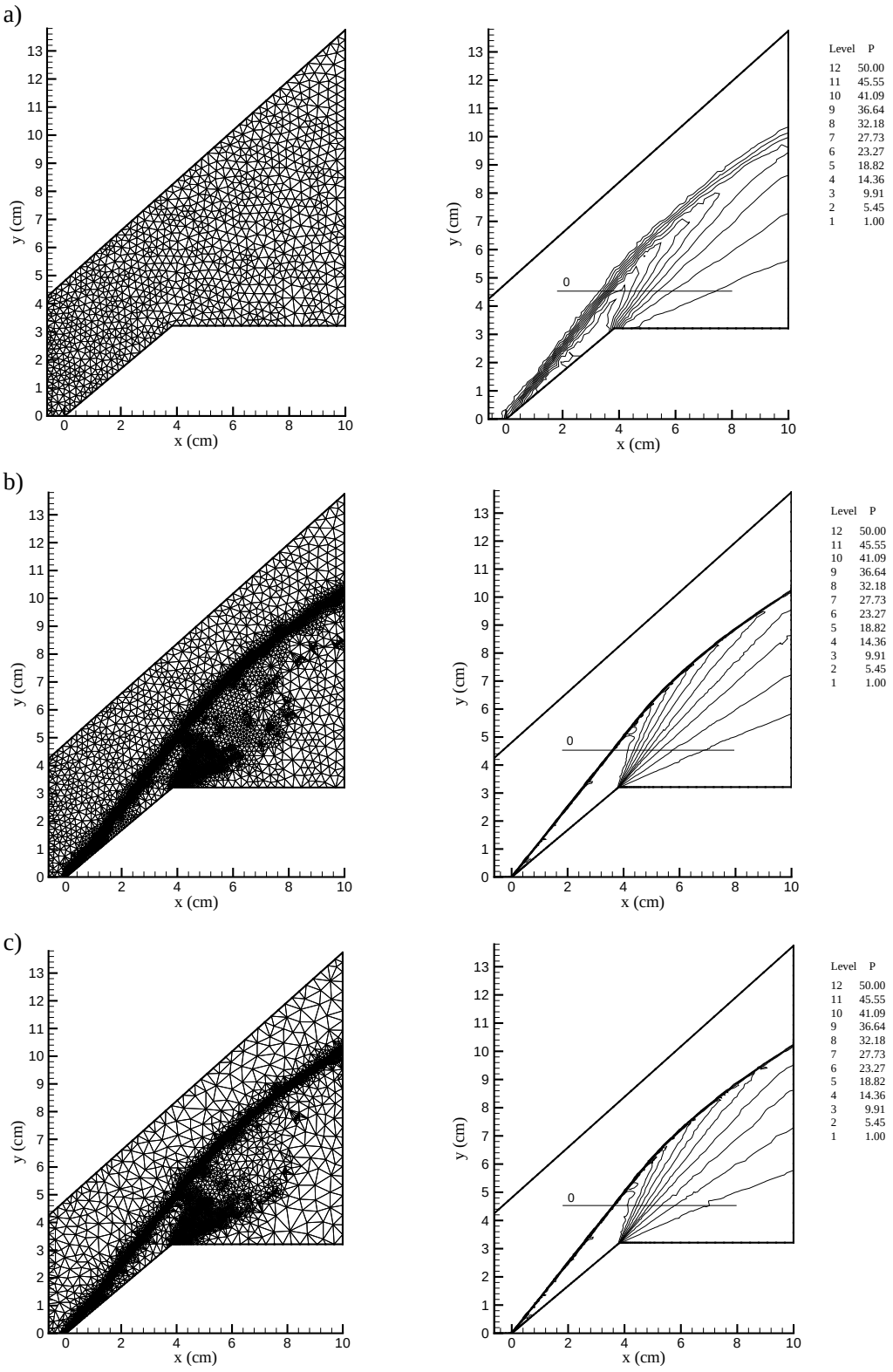

Figure 9: Mesh and pressure field (atm) corresponding to the airflow around a compression/expansion ramp, $M_\infty = 8$, $T_\infty = 300$ K and $p_\infty = 1$ atm, wedge angle $\delta = 40°$.

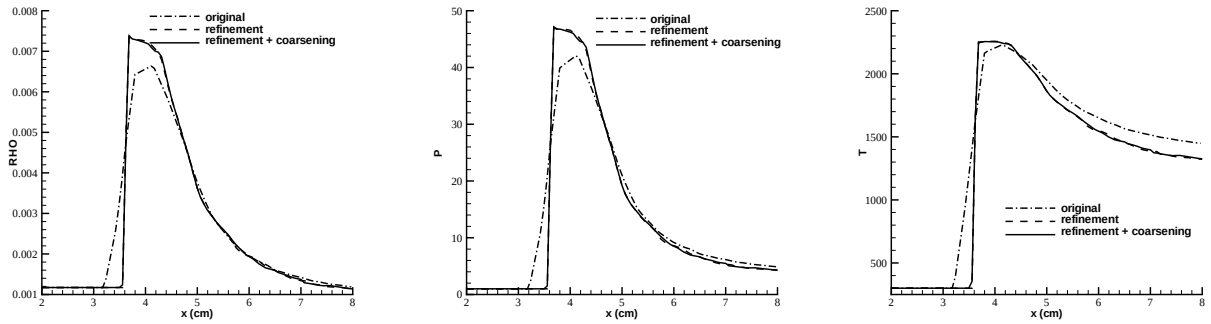

(a) Density (b) Pressure (c) Temperature

Figure 10: Longitudinal evolutions of density (g/cm^3), pressure (atm) and temperature (K) along the line "0" shown in Fig. 9.

illustrated in Fig. 10 by the longitudinal evolution of different flow properties, which are taken along line "0". This figure shows that a clear improvement of the shock wave resolution results when the mesh is refined. Indeed, the values of pressure and temperature predicted by the shock polar analysis (Shapiro, 1983), 47.4 atm and 2325 K, could not be reproduced by the calculation on the initial coarse mesh. After the three refinement passes, the computed values exhibit an excellent agreement with the classical analysis. Moreover, the use of the coarsening procedure does not alter the pressure downstream the oblique shock wave, and only minor differences are observed at the flow expansion region.

7. Acknowledgements

During this work L. F. Figueira da Silva was on leave from *Laboratoire de Combustion et de Détonique, Centre Nacional de la Recherche Scientifique*, France, with a PROFIX scholarship from CNPq-Brazil.

8. References

Dompierre, J., Labbé, P., Garon, A., and Camarero, R., 2000, Unstructured Tetrahedral Mesh Adaptation for Two-Dimensional Space-Time Finite Elements, "38th AIAA Aerospace Sciences Meeting and Exhibit".

Figueira da Silva, L., Azevedo, J., and Korzenowski, H., 1999, On the Development of an Unstructured Grid Solver for Inert and Reactive High Speed Flow Simulations, "RBCM - Jornal of the Brazilian Society of Mechanical Sciences", Vol. XXI, No. 4, pp. 564–579.

Figueira da Silva, L. F., Azevedo, J. L. F., and Korzenowski, H., 2000, Unstructured Adaptive Grid Flow Simulations of Inert and Reactive Gas Mixtures, "Journal of Computational Physics", Vol. 160, No. 2, pp. 522–540.

Hirsch, C., 1990, "Numerical Computations of Internal and External Flows", John Wiley & Sons, Inc., Chichester.

Kallinderis, Y. and Vijayan, P., 1993, Adaptive Refinement-Coarsening Scheme for Three-Dimensional Unstructured Meshes, "AIAA Journal", Vol. 31, No. 8, pp. 1440–1447.

Liou, M.-S., 1996, A Sequel to AUSM: AUSM$^+$, "Journal of Computational Physics", Vol. 129, No. 2, pp. 364–382.

Mavriplis, D., 1988, Two-Dimensional Euler Equations on Unstructured Triangular Meshes, "AIAA Journal", Vol. 26, No. 7, pp. 824–831.

Miller, G. L., Talmor, D., and Tseng, S.-H., 1999, Optimal Coarsening of Unstructured Meshes, "Journal of Algorithms", Vol. 31, No. 1, pp. 29–65.

Pimentel, C. A. R., Azevedo, J. L. F., Figueira da Silva, L. F., and Deshaies, B., 2002, Numerical Study of Wedge Supported Oblique Shock Wave-Oblique Detonations Wave Transitions, "Journal of the Brazilian Society of Mechanical Sciences", Vol. XXIV, No. 3, pp. 149–157.

Shapiro, A. H., 1983, "The Dynamics and Thermodynamics of Compressible Fluid Flow", Robert E. Krieger Publishing Co., Malabar, Florida.

Speares, W. and Berzins, M., 1997, A 3D Unstructured Mesh Adaptation Algorithm for Time-Dependent

Shock-Dominated Problems, "International Journal for Numerical Methods in Fluids", Vol. 25, pp. 81–104.

Walter, M. T. and Figueira da Silva, L. F., 2004, Numerical Study of Detonation Stabilization by Finite Length Wedges, "43rd AIAA/ASME/SAE/ASEE Joint Propulsion Conference and Exhibit".

Webster, B. E., Shephard, M. S., Rusak, Z., and Flaherty, J. E., 1994, Automated Adaptive Time-Discontinuous Finite Element Method for Unsteady Compressible Airfoil Aerodynamics, "AIAA Journal", Vol. 32, No. 4, pp. 748–757.